Improving the wind-induced human comfort of the Beijing Olympic Tower by a double-stage pendulum tuned mass damper

Xin Chen[1]; Aiqun Li[2], Zhiqiang Zhang[3]; Liang Hu[4]; Peng Sun[5]; Zhong Fan[6]; Xianming Liu[7]

Abstract: With five sub towers and a maximum height of 246.8 m, the Beijing Olympic Tower (BOT) is a landmark of Beijing. The complex structural properties and slenderness of the BOT render it prone to wind loading. As far as the wind-induced performance of this structure is concerned, this paper thus aims at a tuned mass damper-based mitigation system for controlling the wind-induced acceleration response of the BOT. To this end, the three-dimensional wind loading of various wind directions are simulated based on the fluctuating wind force obtained by the wind tunnel test, by which the wind-induced vibration is evaluated in the time domain by using the finite element model (FEM). A double-stage pendulum tuned mass pamper (DPTMD), which is capable of controlling the long period dynamic response and requires only a limited space of installation, is optimally designed at the upper part of the tower. Finally, the wind-induced response of the structure with and without DPTMD is compared with respect to various wind directions and in both the time

[1]Associate Professor, Jiangsu Province Key Laboratory of Structure Engineering, Suzhou University of Science and Technology, Suzhou, P.R.China, 215011 (Corresponding author). E-mail: chenx@usts.edu.cn

[2] Professor, Beijing Advanced Innovation Center for Future Urban Design, Beijing University of Civil Engineering and Architecture, Beijing, P.R.China, 100044. E-mail: aiqunli@bucea.edu.cn

[3] Associate Professor, School of Civil Engineering, Southeast Univ., Nanjing, P.R.China, 210096. E-mail: zzq1969@seu.edu.cn

[4] Ph.D Candidtate, NatHaz Modeling Laboratory, University of Notre Dame, Notre Dame, IN 46556. E-mail: peettr@gmail.com

[5] Postdoctoral Research Fellow, Department of Civil and Environmental Engineering, University of Michigan, Ann Arbor, Michigan, 48105. E-mail: patcivil@umich.edu

[6] Professor, China Architecture Design & Research Group, Beijing, P.R.China, 100044. E-mail: fanz@cadg.cn

[7] Professor, China Architecture Design & Research Group, Beijing, P.R.China, 100044. E-mail: liuxm@cadg.cn

and frequency domain. The comparative results show that the wind-induced accelerations atop the tower with the wind directions of 45°, 135°, 225°, and 315° are larger than those with the other directions. The DPTMD significantly reduces the wind-induced response by the maximum acceleration reduction ratio of 30.05%. Moreover, it is revealed that the control effect varies noticeably for the five sub towers, depending on the connection rigidity between Tower1 and each sub tower.

Keyword: Multi-tower structure; Wind-induced responses; Human comfort; Double-stage pendulum tuned mass damper; Vibration mitigation; High-rise building

1. Introduction

With the increasing use of high-strength materials, light-weight floors, and curtain wall systems, the mass and stiffness of modern high-rise buildings and towers are decreasing (Ghorbani-Tanha et al. 2009; Kim et al. 2008). Thus, they suffer from excessive wind-induced oscillations (Chen et al. 2018; Li et al. 2011). The undesirably excessive vibration may cause not only the structural damage or failure but also the discomfort of occupants. Hence, very often those structures may need specific measures to mitigate the wind-induced responses (Kareem et al. 1999). Generally, increasing the structural stiffness is effective in reducing dynamic response, but it is often economically inefficient. Structural control technology, which aims to enhance structural safety and serviceability against dynamic excitations, is now a widely-used alternative (Basu et al. 2014; Spencer&Nagarajaiah 2003; Housner et al. 1997; Soong&Spencer 2002; Ikeda 2009).

Tuned mass damper (TMD) is one of the simplest and practical control devices and especially useful in mitigating dynamic response within the narrow frequency range. Generally, a typical TMD

can be modeled as a device consisting of a mass element, a stiffness element, and a damping element. The frequency of the TMD is tuned to a particular vibration frequency so that when the structural vibration at that frequency is excited, the damper will resonate out of phase and mitigate the induced vibration. A portion of vibration energy input to the structure may be imparted to the TMD and dissipated by the damping element. Due to the convenient implementation procedure, low cost and no requirement of external energy, TMD has attracted many researches, most of which are focused on the configuration, design, and application of the TMD. A proper configuration is essential to realize the TMD in engineering practice. Options of the effective stiffness may include the springs (Ohtake et al. 1992; Chen et al. 2012), the suspended pendulum (Roffel et al. 2013; Nagase&Hisatoku 1992), and the laminated rubber bearings (Saito et al. 2001). Although the oil dampers are typical, there are still others such as the friction (Chung et al. 2013), the eddy current (Lu et al. 2018), the sub tuned absorbers (Sarkar&Gudmestad 2013), and the pounding (Song et al. 2016; Zhang et al. 2013). Moreover, the analysis and design methods of TMD are under active investigation, including the design formulas of the TMD's parameters. These researches may date back to (Den Hartog 1956), such as simplified expressions for optimum TMD parameters of undamped/damped systems considering various combinations of responses (e.g., displacement, velocity, acceleration and force) and excitations (e.g., harmonic and white noise random excitations) (Chang&Qu 1998; Sadek et al. 1997; Warburton 1982; Chung et al. 2013; Hoang et al. 2008; Fujino&Abe 1993). On the other hand, the metaheuristic optimization methods have been utilized in the design of TMD (Farshidianfar&Soheili 2013; Leung et al. 2008; Bekdaş&Nigdeli 2011; Bekdaş et al. 2018; Carlo Marano et al. 2010; Jin et al. 2018).

With the development in the past four decades, the TMD has been successfully installed on

practical buildings to mitigate dynamic responses including pedestrian-induced vibration (An et al. 2015; Chen et al. 2012), wind-induced vibration (Ghorbani-Tanha et al. 2009; Nagase&Hisatoku 1992) and earthquake-induced vibration (Chen et al. 2018; Hoang et al. 2008). Researches and applications show that the TMD in the high-rise tower can suppress the wind-induced vibration significantly, such as John Hancock Tower in Boston (1975), Taipei 101 Tower (Kao et al. 2011), Shanghai Tower (Zhou et al. 2018), and many others (Ghorbani-Tanha et al. 2009; Ohtake et al. 1992; Kang et al. 2012; Li et al. 2011; McNamara 1977; Nagase&Hisatoku 1992). Most of these cases are a TMD on a single-tower building, but most recently some complicated buildings with two or more towers have been constructed out of their architecture benefits. However, the researches of TMD on these irregular buildings are rare. Hence, further investigations on the wind-induced vibration and mitigation are still needed for multi-tower buildings.

With a height of 246.8m, Beijing Olympic Tower (BOT) in the northern of Beijing, China, is a new landmark. The BOT consists of five towers, each of which has an atop large mass. Preliminary studies demonstrate that the upper part of the tower suffers from excessive wind-induced acceleration beyond the human comfortability limit. This paper presents a study on the TMD installed on the BOT. The remainder of this paper is organized as follows. Section 2 introduces the structural system of the BOT. Section 3 presents the finite element model (FEM) of the structure and discusses its dynamic characteristics. The following section introduces the results of the wind tunnel test for this structure and the simulation of the wind loading in the time domain. Section 5 designs a double-stage pendulum tuned mass damper (DPTMD) for this tower and assesses the mitigation effect of the tower by comparing the acceleration response with and without the DPTMD. Finally, the main conclusions of the numerical study are summarized in Section 6.

2. Description of the Beijing Olympic Tower

Beijing Olympic Tower (BOT), shown in Fig.1, is adjacent to the landscape avenue on the axis line of the Beijing Olympic Forest Park. It boasts one of the two buildings around the world officially with Olympic rings permanently on the top (BeijingInternational 2016; OlympicNews 2016). This tower consists of five sub towers with different heights: one central tower (Tower1) locates in the middle and four lower towers (Tower2, Tower3, Tower4, and Tower5) stands around the Tower1. The geometry of these sub towers is shown in Table.1. Towers 2-5 are connected to Tower1 by the corridors which are spatial steel girders with a height of 3.0m and a width of 2.7m. The sections of these sub towers are regular hexagon or circular, the dimension of which increases with the height. The structure of Tower1 is a tube-in-tube system; its outer tube is composed of 16 concrete-filled steel tube (CFST) circular columns stiffened by I-shape steel beams and H-shape steel braces. Towers 2-5 has the structure of tube systems composed of 6 CFST circular columns connected by steel beams and braces.

3. Dynamic characteristics of the structure

3.1 Finite element model

As shown in Fig.2, a three-dimensional (3D) finite element model (FEM) of the BOT was established by using CSI SAP2000 based on the structural design drawings. Two kinds of elements were employed in the FEM: the beam elements for the beams, columns, and braces, and the shell elements for the floors and walls. The nonstructural components were modeled as the dead loads, while the mass was transformed from the dead loads and live loads. The connections between the braces and other components were hinged constraints, and the connections between the beams and columns and between the structure and its foundation were fixed constraints.

3.2 Natural frequencies and modal shapes

The structural dynamic characteristics of the BOT were analyzed and shown in Table.2 and Fig.3. Here, 45° and 135° denotes the angles between the vibration directions and the *x*-axis in the *x*-*y* plane. It can be observed that the first natural period can be as long as 5.687s and the torsional-translation period ratio is 0.775. The first two modes of the tower are overall bending in the direction of 45° and 135°, respectively, where the third mode is torsional. The first six modes are overall vibration modes, indicating that the corridors in this tower are stiff enough to combine the five sub towers. The modes from the sixth to ninth are all 2nd order torsional modes with different vibration shapes of the sub towers with dense-distributed frequencies, which may influence the vibration of the tower.

4. Wind loads simulation

4.1 Introduction of the wind tunnel test

Wind tunnel testing is an effective tool to evaluate the wind effects on buildings, especially those with complex silhouettes. In this study, wind tunnel tests of wind pressure on the BOT were carried out in the atmospheric boundary layer wind tunnel TJ-2 at the Tongji University using a synchronous multi-pressure sensing system (Ming et al. 2010). The dimension of the working section of the wind tunnel is 3.0m wide ×2.5m high. In order to reproduce the building shape more detailed, the rigid sectional models are used. The whole building is divided into four sections vertically. The sectional models are made of plexiglass and ABS. These four scaled segments are shown in Fig.4(a), and the tower bodies and the tower crowns are 1:70 and 1:100 scaled, respectively. The wind direction is defined as an angle from the tower south along a clockwise direction (see Fig.4(b)), and the measurements were made with the wind direction varying from 0° to 360° with the increment of

15°. 1944 pressure taps were installed on these four sectional models. Due to the lack of instruments, the scaled are divided into eight synchronous pressure measuring segments, and not all of them use the same sampling rate. Hence, the pressure data were acquired at five sampling rates with a sampling length of 6000 steps. The sectional model testing was conducted in a turbulent wind field with the turbulence intensity in Table.3, but the mean wind speed was 12.0 m/s and constant along the height. In this experiment, significant mutual aerodynamic interference effects among the sub towers existed, and complicated wind pressure and force distributions were found. Therefore, the wind loads for the BOT is undoubtedly different from the conventional high-rise towers.

4.2 Simulation of the three-dimensional wind loads

In this paper, because of the nonlinearity of the damping devices, the time-domain method is introduced to compute the wind-induced vibration of the BOT. To this end, one should simulate a three-dimensional wind loading field that is applicable to the FEM of the BOT firstly. In this study, the fluctuating wind pressure coefficients given by the wind tunnel tests are used to model the three-dimensional wind field. However, there are some difficulties to utilize these data directly: (1) As mentioned above, the data were acquired at five different sampling rates, including 6.0391Hz, 8.1145 Hz, 7.3379 Hz, 6.8065 Hz, and 6.2723 Hz. (2) The directions of the tested wind pressure coefficients are perpendicular to the model surfaces. (3) There are 1944 pressure taps and 6000 steps per testing wind direction, and locations of the pressure taps do not strictly one-to-one coincide with the structural nodes in the FEM. These difficulties may lead to unsynchronized time steps, difficulty in the loads' assignment and extensive computing time in the FEM time history analysis. Therefore, a method for the three-dimensional wind loading field simulation is proposed as depicted by Fig.5 including four steps:

(1) In order to unify the sampling rates of all data into 6.0391Hz, the nearest interpolation method is used. Fig.6 shows the comparison of the data from a pressure tap with and without interpolation and illustrates a good agreement not only in the time domain but also in the frequency domain.

(2) The wind pressure coefficients are decomposed into three orthogonal directions based on the global coordinate system of the FEM. Hence, the wind pressure coefficients in the *x*, *y,* and *z*-direction of global coordinate can be obtained as follows:

$$\mu_{si,x}(t) = \mu_{si}(t) \cdot \cos\varphi \cdot \sin\theta \tag{1}$$

$$\mu_{si,y}(t) = \mu_{si}(t) \cdot \cos\varphi \cdot \cos\theta \tag{2}$$

$$\mu_{si,z}(t) = \mu_{si}(t) \cdot \sin\varphi \tag{3}$$

where μ_{si} is the wind pressure coefficient of the *i*th pressure tap; $\mu_{si,x}$, $\mu_{si,y}$ and $\mu_{si,z}$ are the decomposed wind pressure coefficients in the *x*, *y*, and *z*-direction of the *i*th pressure tap; φ and θ, shown in Fig.5, are the angles between the normal direction of the surface and the horizontal and vertical axis direction respectively.

(3) The surface of the tower is divided into 1367 sub-areas in which the values of the wind pressure coefficients of the embodied pressure taps are regarded as the same. In each subarea, the nominal wind pressure coefficients can be calculated as:

$$\mu_{sk} = \frac{\sum_{i=1}^{n} A_i \mu_{si}}{\sum_{i=1}^{n} A_i} \tag{4}$$

where μ_{sk} is the wind pressure coefficient of the *k*th subarea, A_i is the influence area of *i*th pressure tap, *n* is the total number of the pressure taps included in the *k*th area. Then the wind pressure of the *k*th subarea can be written as:

$$w_k(t) = \mu_{sk}(t)\mu_{zk}w_0 \tag{5}$$

where w_k is the wind pressure of the kth subarea, μ_{zk} is the height coefficients of the wind pressure, w_0 is the basic wind pressure, in this study w_0=0.30 kPa according to 10-year return period (2012). Both the Eqs. (4) and (5) applies to x, y, and z-direction.

(4) Lastly, the loading nodes in the FEM are selected for the subareas in Step (3), and the wind loading time histories can be calculated as:

$$F_m(t) = w_k(t)A_m \tag{6}$$

where F_m is the mth loading nodes, A_m is the influence area of the mth loading nodes. Finally, 4101 time histories in FEM global coordinate system are obtained.

5. Vibration control using DPTMD

5.1 Design of the Double-stage Pendulum Tuned Mass Damper

A TMD system is installed in the BOT in order to mitigate the excessive wind-induced vibration. Constrained by the architectural requirements, the space available for the mitigation service in this building is quite limited: only a room of 4.80m×4.20m×5.80m can be utilized. In order to take full advantage of the space without a significant increase in the total weight, the fire water tank is utilized as the mass element of the absorber, because the volume of the tank excludes the possibility as a sloshing-based mitigation. In consideration of all these factors, a Double-stage Pendulum Tuned Mass Damper (DPTMD) was designed and installed on the floor of the Tower1 at the height of 232.5m(Fig.7).

There are some requirements, including long period, limit space and all motion directions, for the TMD used in this tower. If a conventional pendulum TMD scheme was used in this project, at least a space with more than 7.90m in height should be needed. However, the height of the available space for the TMD is only 5.80m. Therefore, this DPTMD system utilizes the fire water tank as the

mass element and hangs the tank by a double-stage suspension system. As shown in Fig.8, this system is composed of the fire water tank, outer cables, inner cables, suspension frame, tank support, viscous dampers, limiters, structure connections, and support connections. The tank support supports the fire water tank, which has a total mass of 50t. They together are hung by the double-stage suspension system consisting of the outer cables, inner cables, and suspension frame. Four viscous dampers are installed between the floor and the tank support to suppress the motion between the tank and its support. Moreover, four limiters are used to restrict the maximum displacement of the tank. The parameters of the DPTMD are shown in Table.4, determined by the limitations of the total mass, maximum stroke and installation space of the DPTMD. The mass ratio of the DPTMD to the structure is only 0.058%. The frequency ratio of the DPTMD in the directions of the first two modes are 1.055 and 1.025, while the corresponding damping ratios are 0.120 and 0.116 respectively. Considering the uncertainty in the construction, one can adjust the length of the cables after the field testing.

5.2 Numerical simulation of the wind-induced vibration

5.2.1 Spatial distribution

The wind-induced vibrations of the BOT with and without TMD are analyzed by inputting the three-dimensional wind field simulated in Section 4.2 to the FEM model. Fig.9 shows the spatial distribution of the maximum node acceleration over time under the wind directions of 45° and 135°. The combination of the horizontal accelerations and of all the three acceleration components are $\sqrt{a_x^2+a_y^2}$ and $\sqrt{a_x^2+a_y^2+a_z^2}$, in which a_x, a_y, and a_z are the maximum node accelerations over time in the directions of X, Y and Z. It can be observed that: (1) The acceleration distributions of the BOT with and without TMD are similar. After the installation of the TMD, the total horizontal

accelerations are all reduced. However, the TMD does not affect the vertical acceleration responses. (2) In general, the acceleration increases from the bottom to the top and from the inner part to the outer part. The accelerations of the tower crown are larger than those of the body, especially in the vertical direction. The maximum accelerations the main bodies of the Tower 2 and 4 are larger than those of the other sub towers, while those of the crowns of the Tower 3 and 5 are larger than the other towers.

5.2.2 Response variation with wind directions

There are two main public scenic sites in each sub tower: one is the viewing platform at the top of each tower, and the other is the viewing hall, which is the floor immediately below the platform. As there will be many people on these sites to watch the scenery of Beijing city, the issue of human comfort is of concern. Therefore, by considering eight typical wind directions, the mean and maximum horizontal accelerations of the viewing platform and hall are assessed and shown in Fig.10 and Fig.11. It can be concluded from the Fig.10 that: (1) In general, the maximum acceleration occurs at the edge nodes of the viewing platform. The structural constraint on these nodes is much weaker than those at the middle. Thus the reduction effect of the TMD on the mean accelerations is better than on the maximum accelerations. (2) The wind-induced accelerations of the tower subjected to the wind loads with the directions of 45°, 135°, 225°, and 315° are larger than those subjected to the wind loads with the other directions. This phenomenon is mainly due to the first two modal shapes of the BOT. (3) The best reduction effect is with the wind direction of 270°, when the reduction ratio of Tower1, Tower2, and Tower3 are 16.44%, 30.05%, and 22.63%, respectively. (4) Because the DPTMD was installed only on Tower1, it has a slight effect on some of the sub towers, among which reduction effect on Tower5 is limited. The reduction effect in the viewing hall as

shown in Fig.11 is similar to the effect in the viewing platform. Moreover, the maximum reduction ratio of the viewing hall is 24.56%, which also occurs in the wind direction of 270°. As the connections between Tower1 and Tower5 are weaker than those between Tower1 and the other sub towers, the acceleration reduction effect, both in the viewing platform and in the viewing hall of Tower5, is the weakest among these sub towers. Moreover, the reduction effect in the viewing hall is much better than in the viewing platform.

5.2.3 Response time history and PSD

The time history responses and the corresponding power spectral densities of two nodes on the viewing platform of the Tower1 and Tower5 in the *x*-direction are shown in Fig.12 and Fig.13 with the wind direction of 45°. Meanwhile, these responses in the *y*-direction are shown in Fig.14 and Fig.15. In the time domain, the reduction of the displacements is better than the accelerations at both *x* and *y* directions. In the frequency domain, the DPTMD has a considerable reduction effect on both the accelerations and displacements at the first bending mode but does not affect the higher modes. However, the higher modes do have some influences on the wind-induced responses, and the accelerations are affected much more than the displacements. Comparing with the node in Tower 5, the reduction effect of the node in Tower1 is much better, and this confirms the conclusions from the analysis in the section above.

6. Concluding remarks

The wind-induced response of the BOT and the performance of its vibration control are presented in this paper. The three-dimensional wind loading for the FEM analysis of the BOT is established based on the wind tunnel test results. Moreover, based on the dynamic characteristics and responses of the BOT, a DPTMD was designed and installed on the tower. Then, the wind-induced

responses of the tower with and without DPTMD are compared with respect to various wind directions and both in the time and frequency domain. Based on the results and discussions presented, the following remarks can be obtained:

(1) Mostly, the wind-induced accelerations of the tower subjected to the wind loads with the directions of 45°, 135°, 225°, and 315° are larger than those with the other directions.

(2) The DPTMD design utilizes a shorter pendulum length to achieve a long period, thus a lot of spatial space can be saved given the excellent control performance on the BOT can be ensured. The design serves as a reference for other slender high-rise towers.

(3) Only with 0.058% structural mass does the DPTMD mitigate the wind-induced vibration of the tower effectively. The maximum acceleration reduction ratio for the mean accelerations of each floor, which occurs in Tower2 with the wind direction of 270°, reaches 30.05%. Because of the relatively weak connections between sub towers, the reduction effect of the Tower5 is lower than the other sub towers.

(4) Because of the limitation of the physical space, only one TMD with a small mass can be installed in this tower. Only the response induced by the first two modes can be suppressed, although higher modes can affect the towers' wind-induced accelerations as well.

Acknowledgments

The support from the Natural Science Foundation of China under Grant No. 51408389, the Natural Science Foundation of Jiangsu Province under Grant No. BK20161581 and BK20181078, the Six Talent Climax Foundation of Jiangsu under Grant No. JZ-004, the Natural Science Foundation of Jiangsu Education Department under Grant No. 19KJA430019, Jiangsu Government Scholarship for

Overseas Studies and A Project Funded by the Priority Academic Program Development of Jiangsu Higher Education Institutions is gratefully acknowledged.

REFERENCES

(1975). "Hancock Tower now to get dampers." Engineering News Records, 11.

GB50009-2012,(2012)."Load code for design of building structures".Beijing:China Architecture & Building Press.

A. Farshidianfar& S. Soheili. (2013). Optimization of tmd parameters for earthquake vibrations of tall buildings including soil structure interaction. *International Journal of Optimization in Civil Engineering*, 3(3): 409-429.

A. J. Roffel, S. Narasimhan& T. Haskett. (2013). Performance of pendulum tuned mass dampers in reducing the responses of flexible structures. *Journal of Structural Engineering-ASCE*, 139(12): 04013019.

A. K. Ghorbani-Tanha, A. Noorzad& M. Rahimian. (2009). Mitigation of wind-induced motion of milad tower by tuned mass damper. *Structural Design of Tall and Special Buildings*, 18(4): 371-385.

A. Kareem, T. Kijewski& Y. Tamura. (1999). Mitigation of motions of tall buildings with specific examples of recent applications. *Wind and Structures*, 2(3): 201-251.

A. Sarkar& O. T. Gudmestad. (2013). Pendulum type liquid column damper (PLCD) for controlling vibrations of a structure–theoretical and experimental study. *Engineering Structures*, 49: 221-233.

A. Y. T. Leung, H. Zhang& C. C. Cheng, et al. (2008). Particle swarm optimization of TMD by non‐stationary base excitation during earthquake. *Earthquake Engineering & Structural Dynamics*, 37(9): 1223-1246.

B. Basu, O. S. Bursi& F. Casciati, et al. (2014). A European Association for the Control of Structures joint perspective. Recent studies in civil structural control across Europe. *Structural Control and Health Monitoring*, 21(12): 1414-1436.

B. Chen, D. Yang& Y. Zheng, et al. (2018). Response control of a High-Rise television tower under seismic excitations by friction dampers. *International Journal of Structural Stability and Dynamics*, 18(11): 1850140.

B. F. Spencer& S. Nagarajaiah. (2003). State of the art of structural control. *Journal of Structural Engineering-ASCE*, 129(7): 845-856.

BeijingInternational. (2016). Permanent olympic symbol marks beijing's new landmark<http://www.ebeijing.gov.cn/feature_2/SportsinBeijing/t1438765.htm>. June, 19,2019.

C. C. Chang& W. L. Qu. (1998). Unified dynamic absorber design formulas for wind-induced vibration control of tall buildings. *Structural Design of Tall and Special Buildings*, 7(2): 147-166.

C. Kao, A. Y. Tuan& Q. S. Li, et al. (2011). Dynamic behavior of taipei 101 tower: Field measurement and numerical analysis. *Journal of Structural Engineering*, 137(1): 143-155.

F. Sadek, B. Mohraz& A. W. Taylor, et al. (1997). A method of estimating the parameters of tuned mass dampers for seismic applications. *Earthquake Engineering & Structural Dynamics*, 26(6): 617-635.

G. B. Song, P. Zhang& L. Y. Li, et al. (2016). Vibration control of a pipeline structure using pounding tuned mass damper. *Journal of Engineering Mechanics*, 142(6): 04016031.

G. B. Warburton. (1982). Optimum absorber parameters for various combinations of response and excitation parameters. *Earthquake Engineering & Structural Dynamics*, 10(3): 381-401.

G. Bekdaş& S. M. Nigdeli. (2011). Estimating optimum parameters of tuned mass dampers using harmony search. *Engineering Structures*, 33(9): 2716-2723.

G. Bekdaş, S. M. Nigdeli& X. Yang. (2018). A novel bat algorithm based optimum tuning of mass dampers for improving the seismic safety of structures. *Engineering Structures*, 159: 89-98.

G. Carlo Marano, R. Greco& B. Chiaia. (2010). A comparison between different optimization criteria for tuned

mass dampers design. *Journal of Sound and Vibration*, 329(23): 4880-4890.
G. Ming, P. Huang& L. Tao, et al. (2010). Experimental study on wind loading on a complicated group-tower. *Journal of Fluids and Structures*, 26(7-8): 1142-1154.
G. W. Housner, T. K. Caughey& A. G. Chassiakos, et al. (1997). Structural control: Past, present, and future. *Journal of Engineering Mechanics*, 123(9): 897-971.
J. P. Den Hartog. (1956). *Mechanical vibrations*. New York: McGraw-Hill. 492p.
K. Ohtake, Y. Mataki& T. Ohkuma, et al. (1992). Full-scale Measurements of Wind Actions on Chiba Port Tower. *Journal of Wind Engineering and Industrial Aerodynamics*, 41-44: 2225-2236.
L. Chung, L. Wu& C. W. Yang, et al. (2013). Optimal design formulas for viscous tuned mass dampers in wind-excited structures. *Struct. Control Health Monit.*, 20(3): 320-336.
L. L. Chung, L. Y. Wu& K. H. Lien, et al. (2013). Optimal design of friction pendulum tuned mass damper with varying friction coefficient. *Structural Control & Health Monitoring*, 20(4): 544-559.
N. Hoang, Y. Fujino& P. Warnitchai. (2008). Optimal tuned mass damper for seismic applications and practical design formulas. *Engineering Structures*, 30(3): 707-715.
N. Kang, H. Kim& S. Choi Seongwoo Jo, et al. (2012). Performance evaluation of TMD under typhoon using system identification and inverse wind load estimation. *Computer-Aided Civil and Infrastructure Engineering*, 27(6): 455-473.
OlympicNews. (2016). Olympic rings join the beijing skyline<https://www.olympic.org/news/olympic-rings-join-the-beijing-skyline>. June, 19th,2019.
P. Zhang, G. Song& H. Li, et al. (2013). Seismic control of power transmission tower using pounding TMD. *Journal of Engineering Mechanics*, 139(10): 1395-1406.
Q. An, Z. Chen& Q. Ren, et al. (2015). Control of human-induced vibration of an innovative CSBS–CSCFS. *Journal of Constructional Steel Research*, 115: 359-371.
Q. S. Li, L. Zhi& A. Y. Tuan, et al. (2011). Dynamic behavior of taipei 101 tower: Field measurement and numerical analysis. *Journal of Structural Engineering-ASCE*, 137(1): 143-155.
R. J. McNamara. (1977). Tuncd mass dampers for buildings. *Journal of the Structural Division*, 103(9): 1785-1798.
T. Nagase& T. Hisatoku. (1992). Tuned-Pendulum Mass Damper installed Crystal. *The Structural Design of Tall Buildings*, 1: 35-36.
T. Saito, K. Shiba& K. Tamura. (2001). Vibration control characteristics of a hybrid mass damper system installed in tall buildings. *Earthquake Engineering & Structural Dynamics*, 30(11): 1677-1696.
T. T. Soong& B. F. Spencer. (2002). Supplemental energy dissipation: State-of-the-art and state-of-the practice. *Engineering Structures*, 24(3): 243-259.
X. Chen, Y. Ding& Z. Zhang, et al. (2012). Investigations on serviceability control of long-span structures under human-induced excitation. *Earthquake Engineering and Engineering Vibration*, 11(1): 57--71.
X. Jin, S. Xie& J. He, et al. (2018). Optimization of tuned mass damper parameters for floating wind turbines by using the artificial fish swarm algorithm. *Ocean Engineering*, 167: 130-141.
Y. Ikeda. (2009). Active and semi-active vibration control of buildings in Japan-Practical applications and verification. *Structural Control and Health Monitoring*, 16(7-8): 703-723.
Y. Kim, K. You& H. Kim. (2008). Wind-induced excitation control of a tall building with tuned mass dampers. *Structural Design of Tall and Special Buildings*, 17(3): 669-682.
Y. Z. Fujino& M. Abe. (1993). Design formulas for tuned mass dampers based on a perturbation technique. *Earthquake Engineering & Structural Dynamics*, 22(10): 833-854.
Z. Lu, B. Huang& Q. Zhang, et al. (2018). Experimental and analytical study on vibration control effects of eddy-current tuned mass dampers under seismic excitations. *Journal of Sound and Vibration*, 421: 153-165.

365 Z. Zhou, X. Wei& Z. Lu, et al. (2018). Influence of soil-structure interaction on performance of a super tall
366 building using a new eddy-current tuned mass damper. *The Structural Design of Tall and Special Buildings*,
367 27(14): e1501.

368

369 Table.1 Structural geometry of the BOT
370

Tower	Tower1	Tower 2	Tower 3	Tower 4	Tower 5
Architectural diameter/ m	16.20	9.60	9.60	8.30	8.30
Structural diameter/ m	14.00	7.30	7.30	6.00	6.00
Structural height/ m	244.35	228.00	210.00	198.00	186.00
Slenderness ratio	17.45	31.23	28.77	33.00	31.00
Diameter of the top/ m	51.20	33.60	32.40	30.00	26.40
Distance to Tower1/ m	-	19.17	15.75	15.10	16.90

371

372
373 Table.2 Natural frequencies of the tower
374

Modes	Frequency/ Hz	Description
1	0.176	1st overall bending (45°)
2	0.181	1st overall bending (135°)
3	0.227	1st overall torsional (anti-symmetric bending of the Tower2 and 4 (45°) + anti-symmetric bending of the Tower3 and 5 (135°))
4	0.512	2nd overall bending (45°)
5	0.559	2nd overall bending (135°)
6	0.598	2nd overall torsional (symmetric bending of the Tower2 and 4 (45°) + anti-symmetric bending of the Tower3 and 5 (135°))
7	0.703	2nd overall torsional (symmetric bending of the Tower2 and 4 (45°) + symmetric bending of the Tower3 and 5 (135°))
8	0.721	2nd overall torsional (anti-symmetric bending of the Tower2 and 4 (45°) + symmetric bending of the Tower3 and 5 (135°))
9	0.790	2nd overall torsional (local vibration of the Tower4 crown + anti-symmetric bending of the Tower3 and 5 (135°))
10	1.019	3rd overall bending (45°)
11	1.088	3rd overall bending (135°)

375

376
377 Table.3 Simulated turbulence intensity in the model tests
378

Segment model	Elevation/ m	Reference height/ m	Reference turbulence intensity/ %	Simulated turbulence intensity/ %
1	0-49.2	30-40	18-20	18
2	49.2-109.2	70-90	15-16	15
3	109.2-169.2	130-150	13-14	14
4	145.8-244.35	180-200	12	11.5

379

380
381 Table 4. Parameters of the DPTMD system
382

Direction	*x*	*y*
Effective length of cable/ m	7.90	7.90
Mass/ t	50	50
Damping exponent of the damper	1	1
Damping coefficient of the damper/ N·s/m	6997	6788

383
384

TAL_1704_Fig.1a.tif

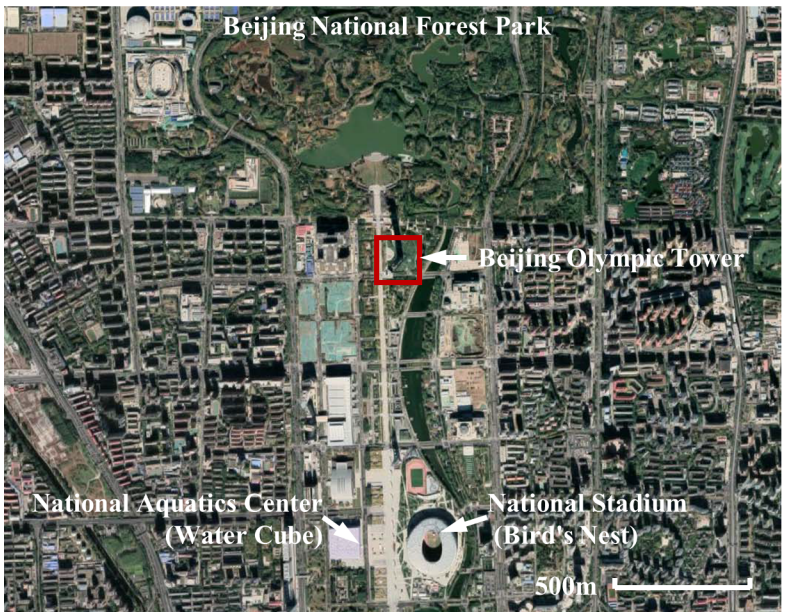

TAL_1704_Fig.1b.tif

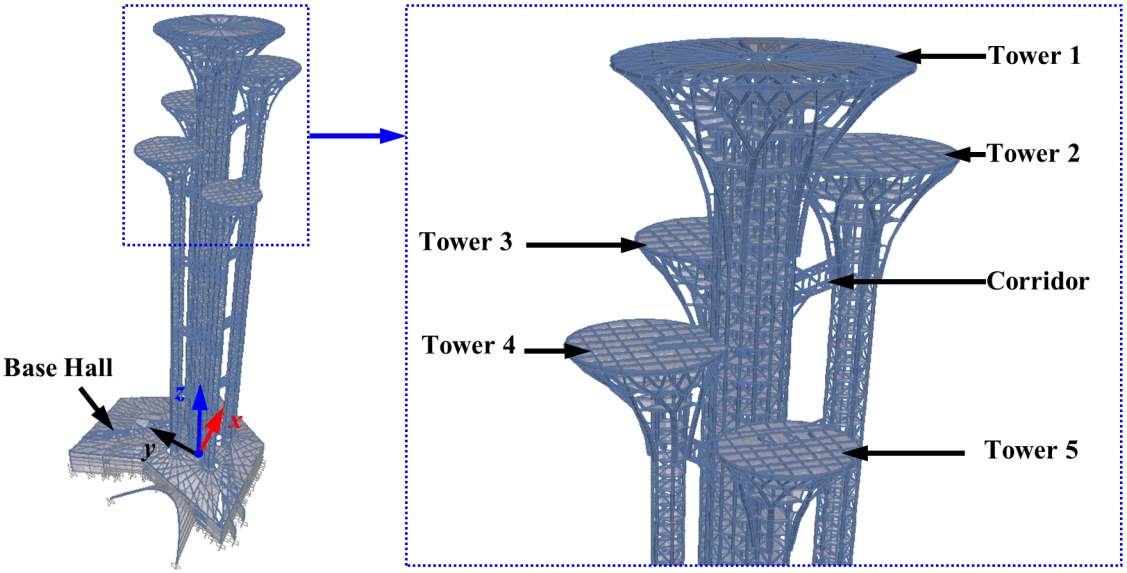

TAL_1704_Fig.2.tif

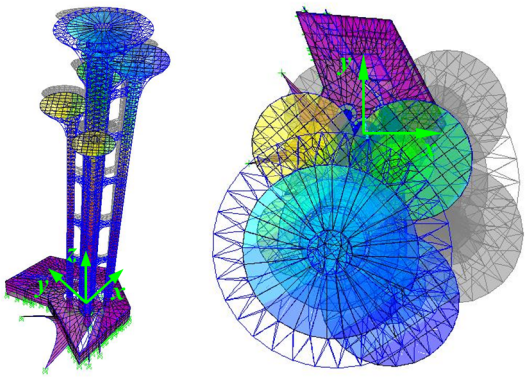

TAL_1704_Fig.3a.tif

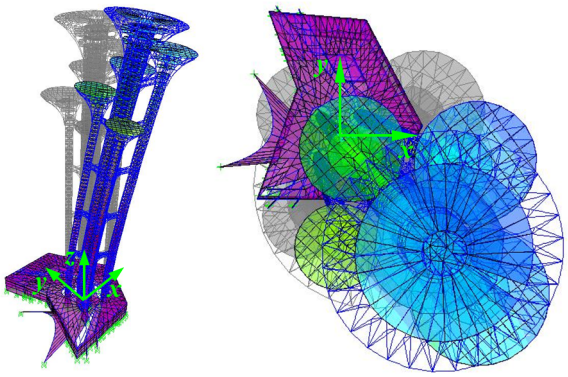

TAL_1704_Fig.3b.tif

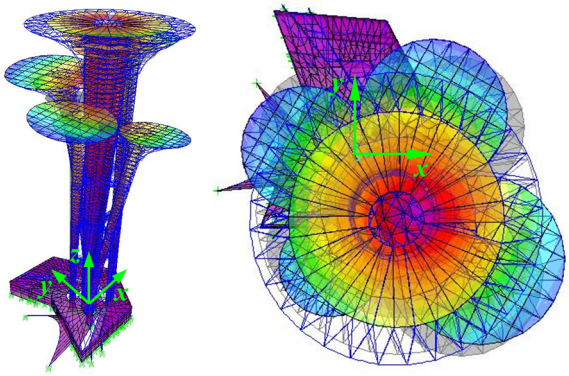

TAL_1704_Fig.3c.tif

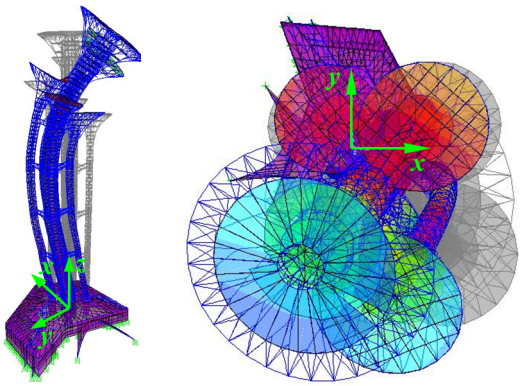

TAL_1704_Fig.3d.tif

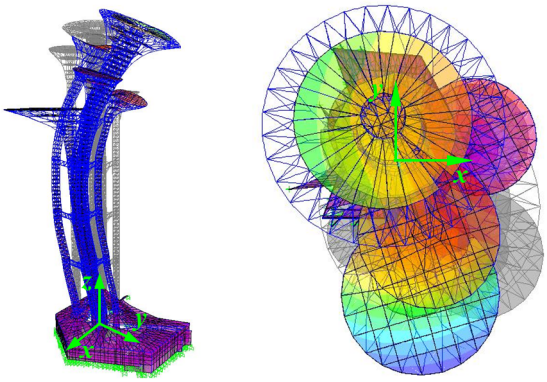

TAL_1704_Fig.3e.tif

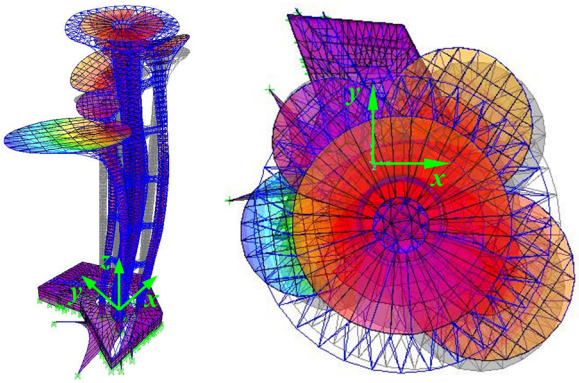

TAL_1704_Fig.3f.tif

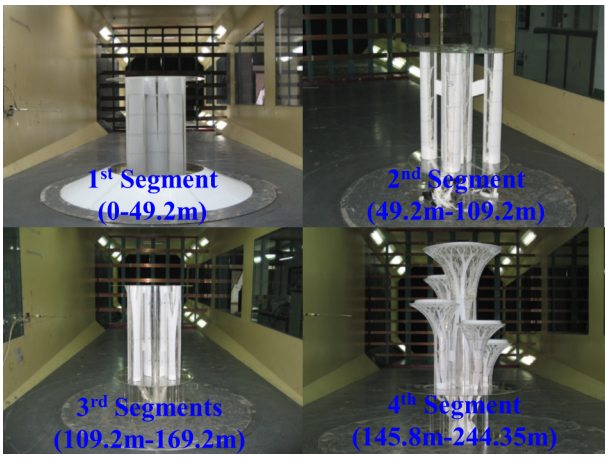

TAL_1704_Fig.4a.tif

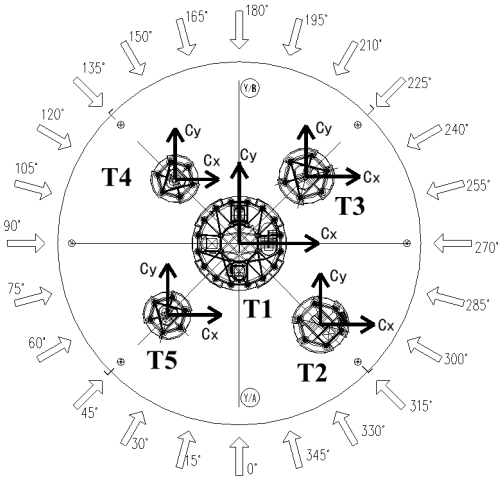

Note: T is short for Tower.

TAL_1704_Fig.4b.tif

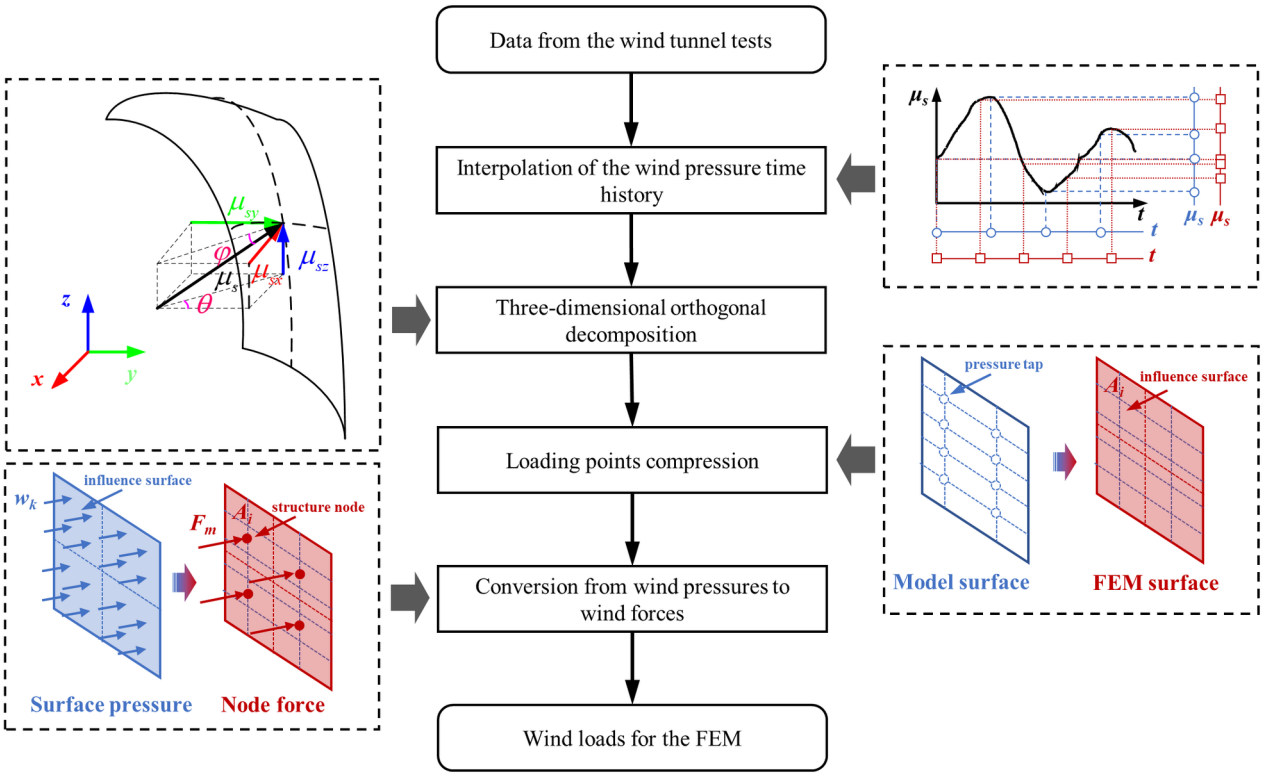

TAL_1704_Fig.5.tif

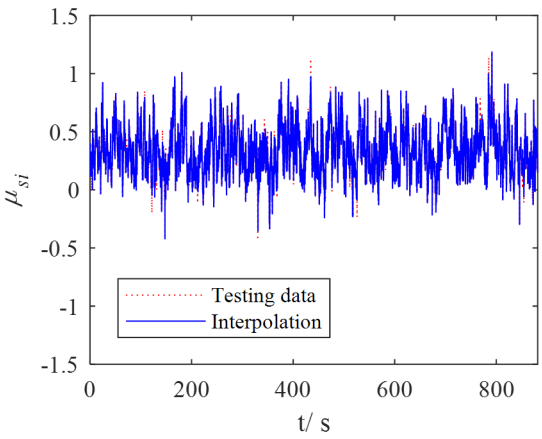

TAL_1704_Fig.6a.tif

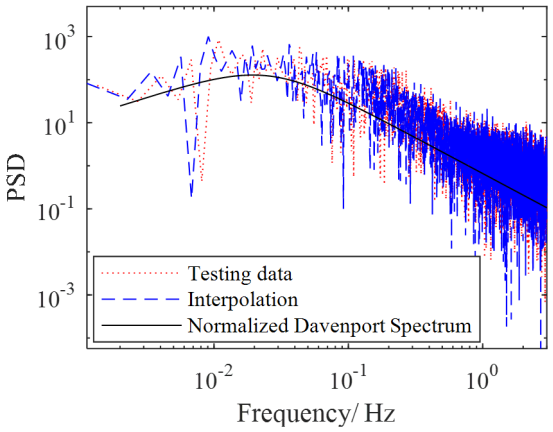

TAL_1704_Fig.6b.tif

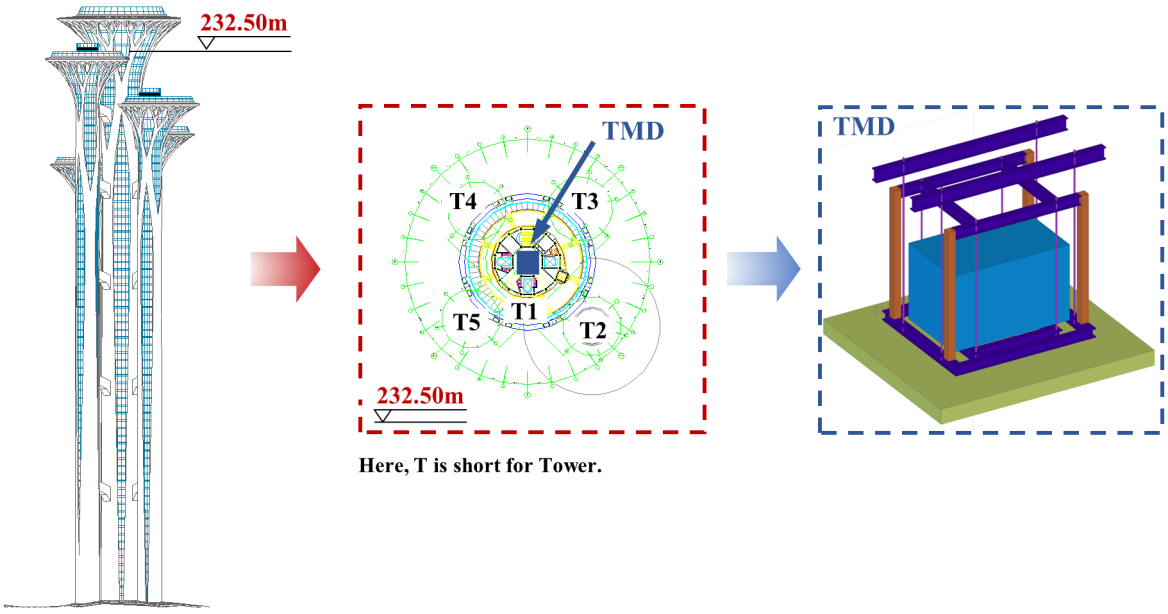

Here, T is short for Tower.

TAL_1704_Fig.7.tif

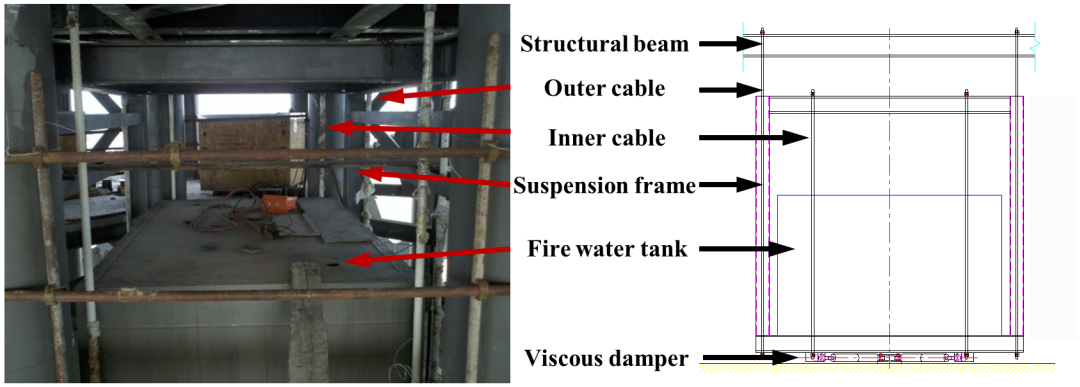

TAL_1704_Fig.8a.tif

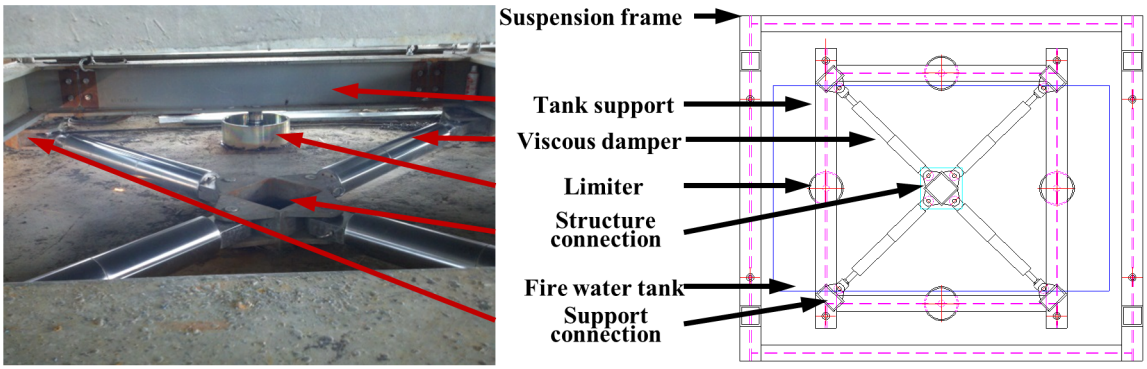

TAL_1704_Fig.8b.tif

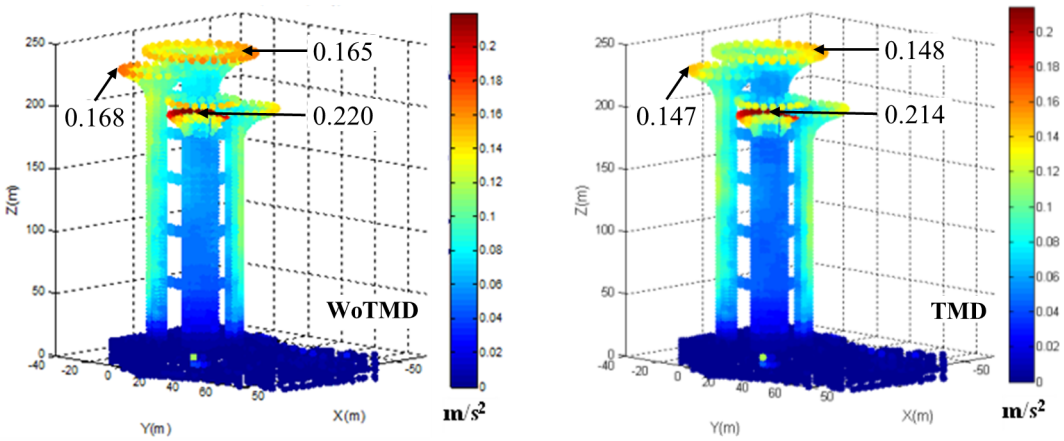

TAL_1704_Fig.9a.tif

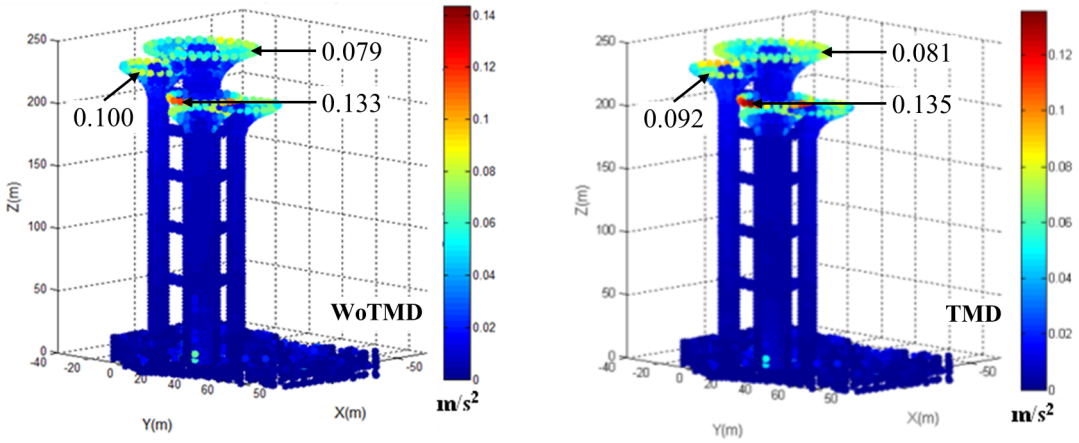

TAL_1704_Fig.9b.tif

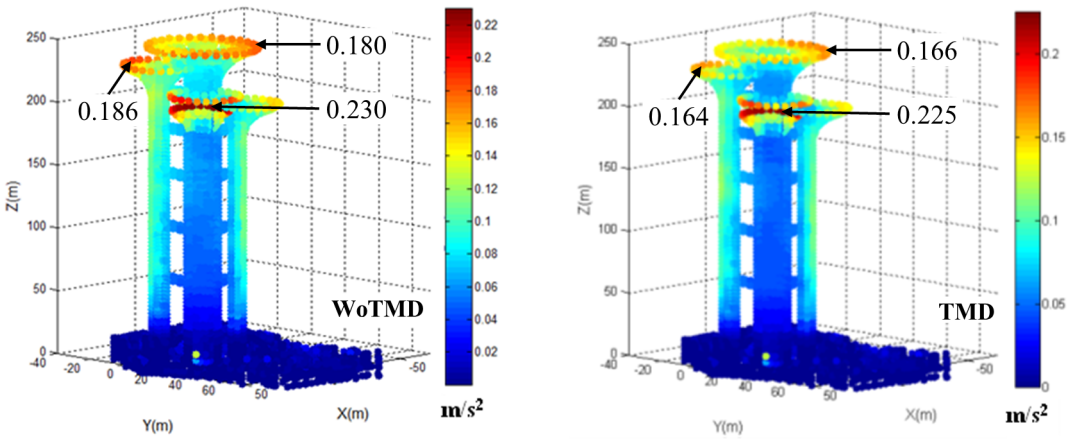

TAL_1704_Fig.9c.tif

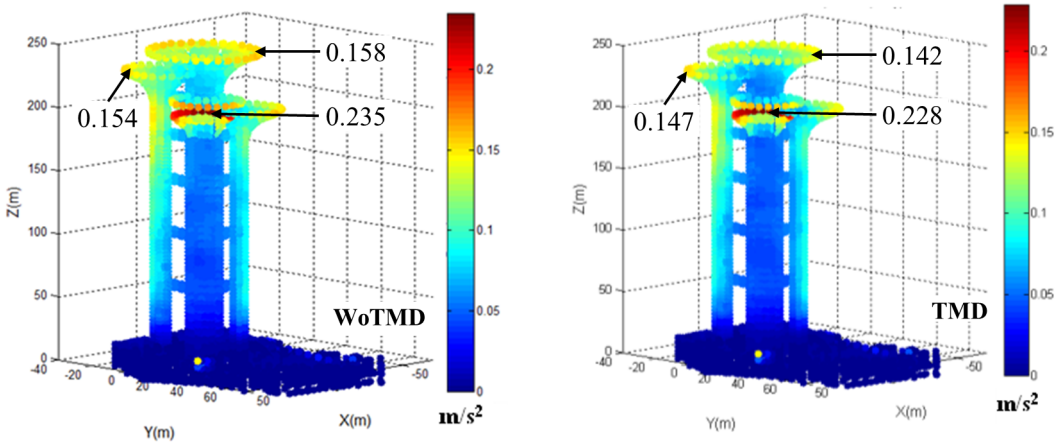

TAL_1704_Fig.9d.tif

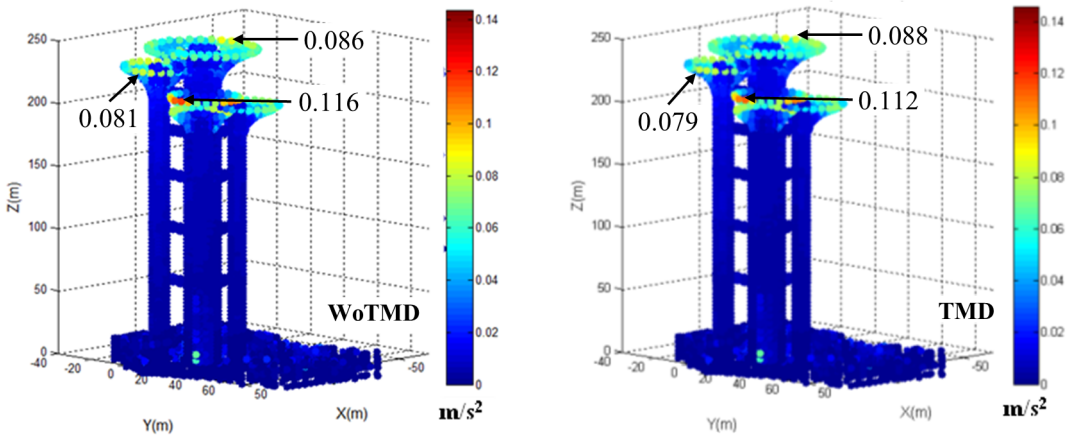

TAL_1704_Fig.9e.tif

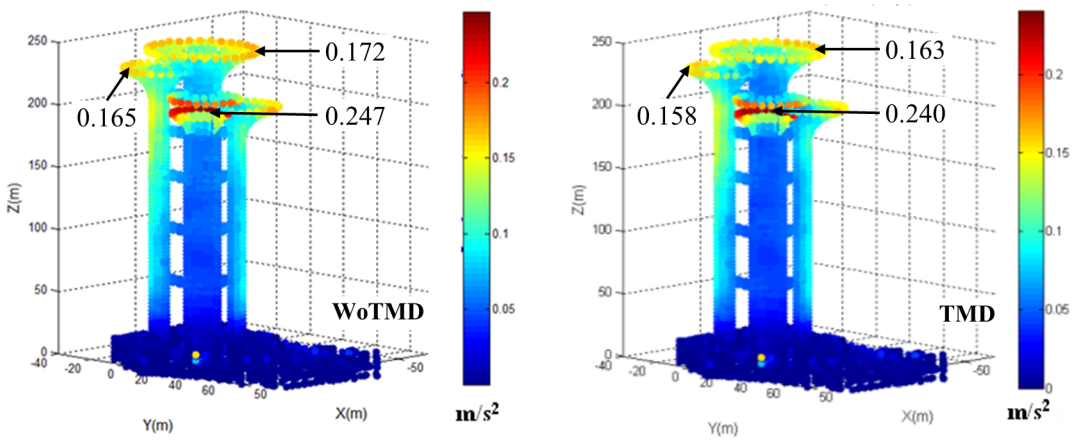

TAL_1704_Fig.9f.tif

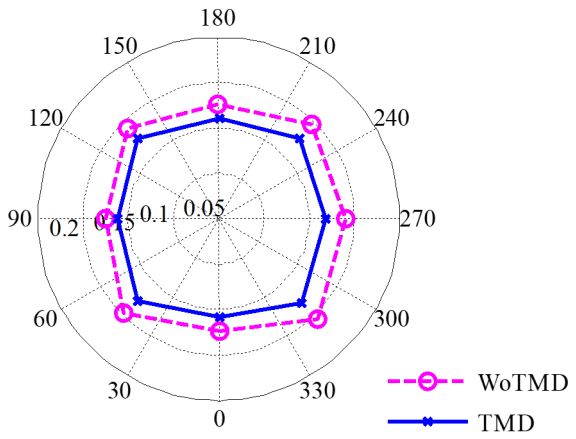

TAL_1704_Fig.10a.tif

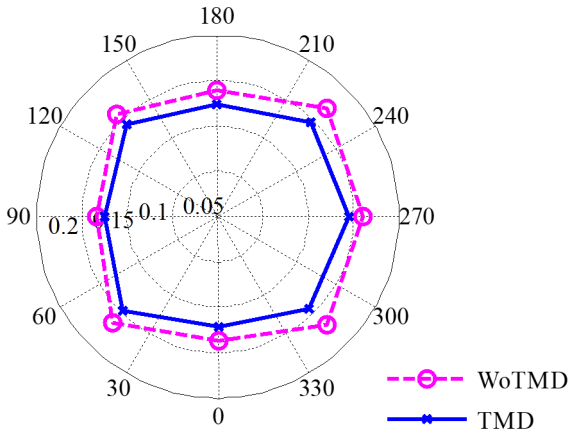

TAL_1704_Fig.10b.tif

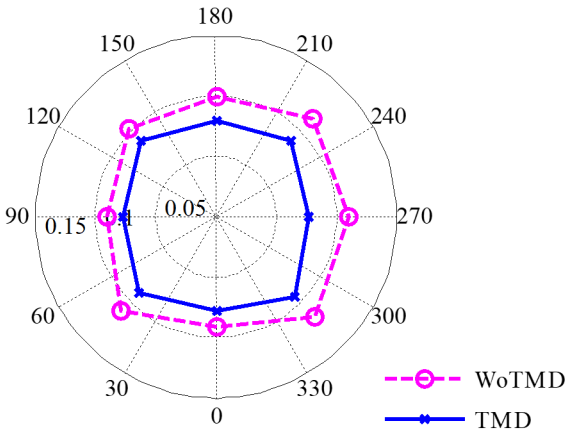

TAL_1704_Fig.10c.tif

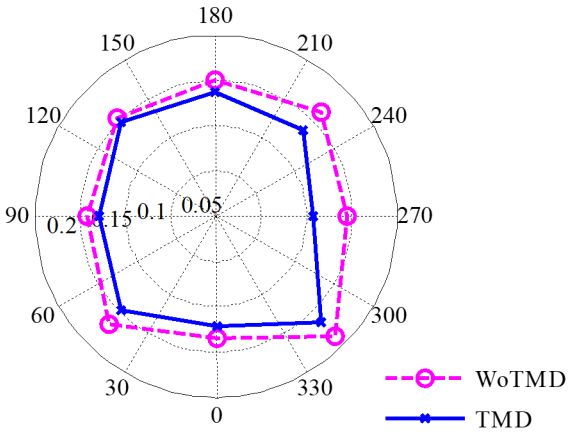

TAL_1704_Fig.10d.tif

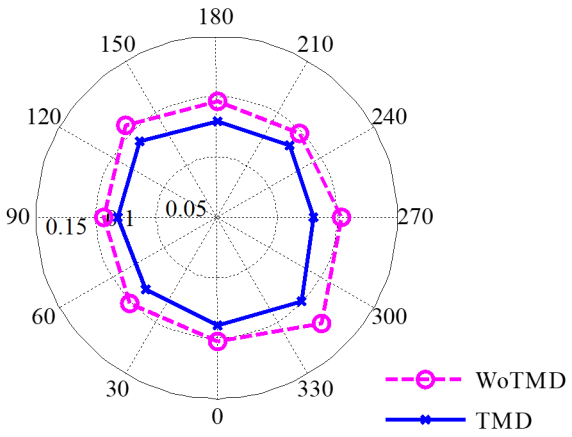

TAL_1704_Fig.10e.tif

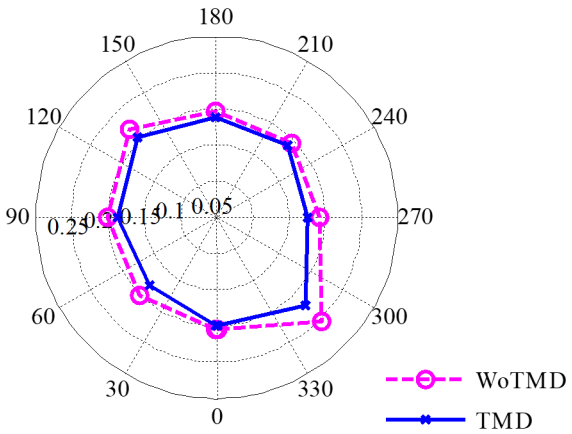

TAL_1704_Fig.10f.tif

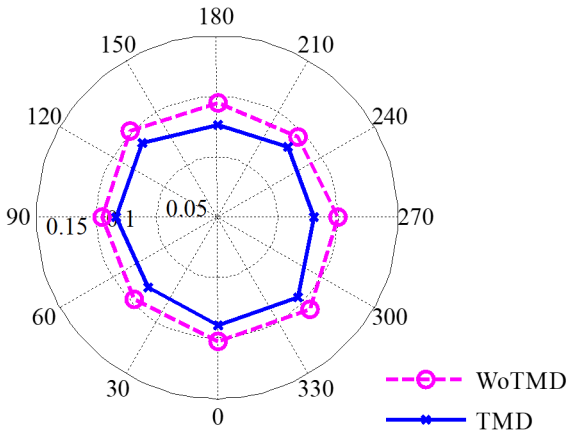

TAL_1704_Fig.10g.tif

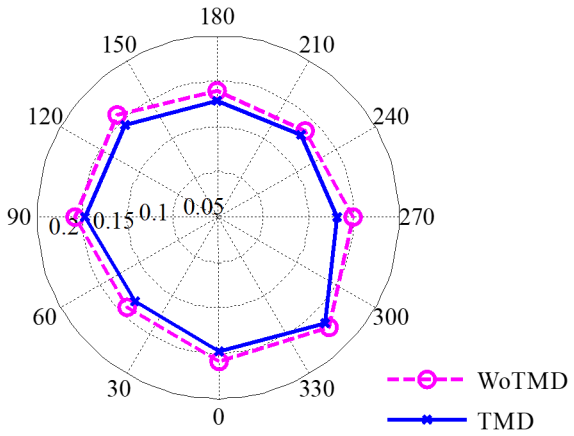

TAL_1704_Fig.10h.tif

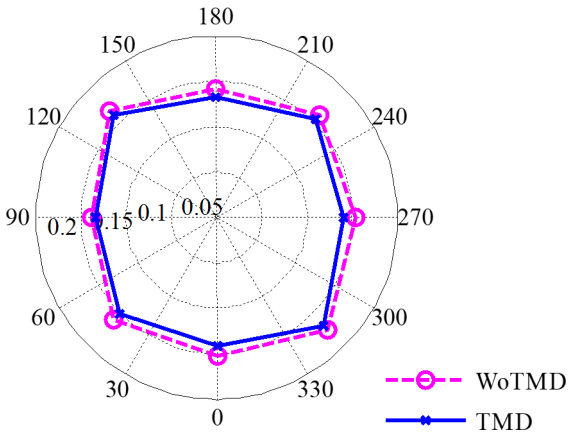

TAL_1704_Fig.10i.tif

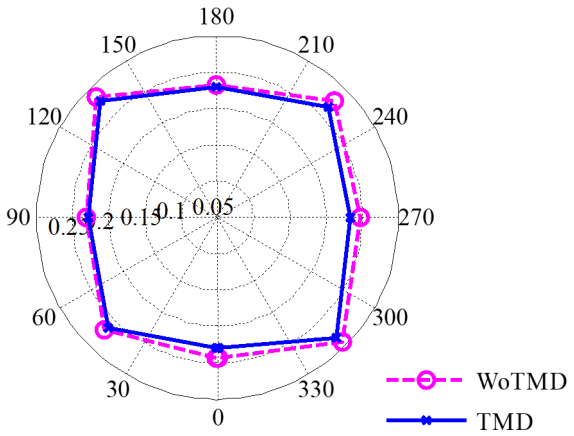

TAL_1704_Fig.10j.tif

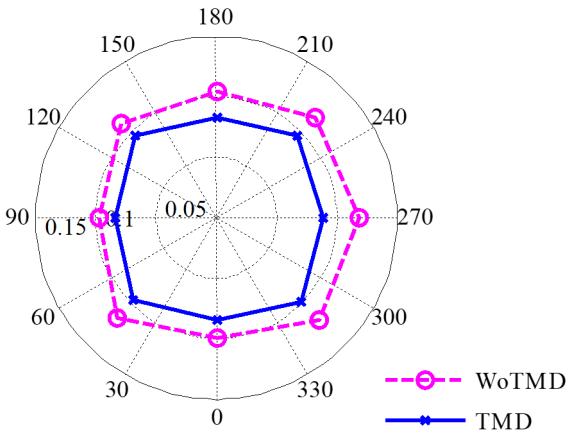

TAL_1704_Fig.11a.tif

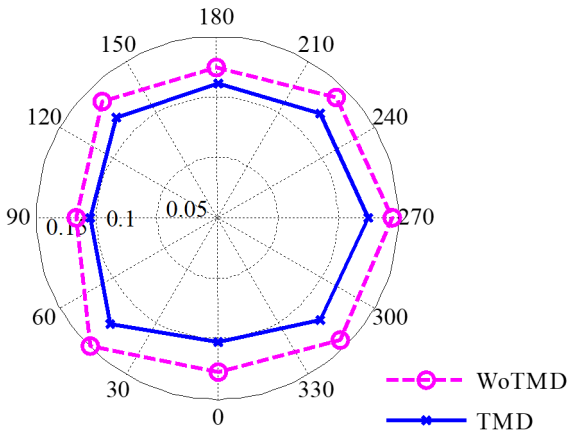

TAL_1704_Fig.11b.tif

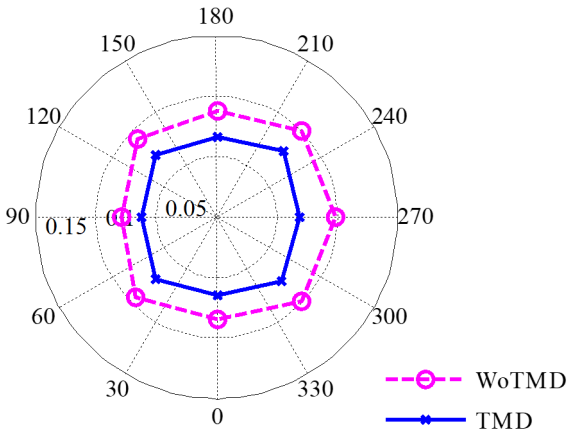

TAL_1704_Fig.11c.tif

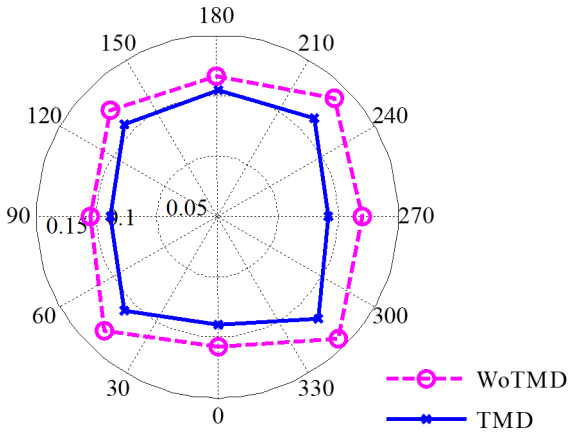

TAL_1704_Fig.11d.tif

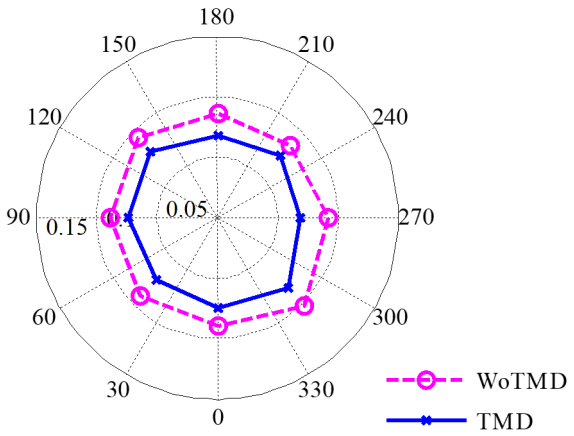

TAL_1704_Fig.11e.tif

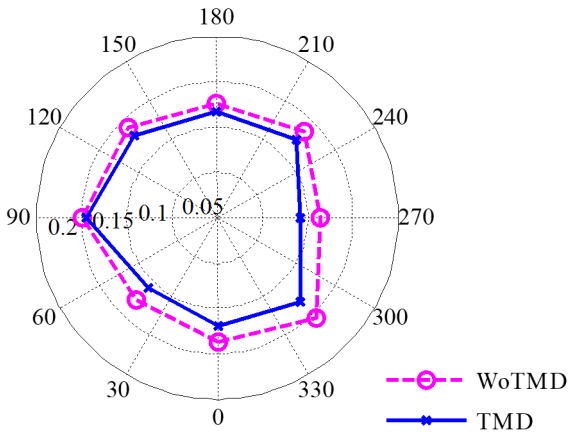

TAL_1704_Fig.11f.tif

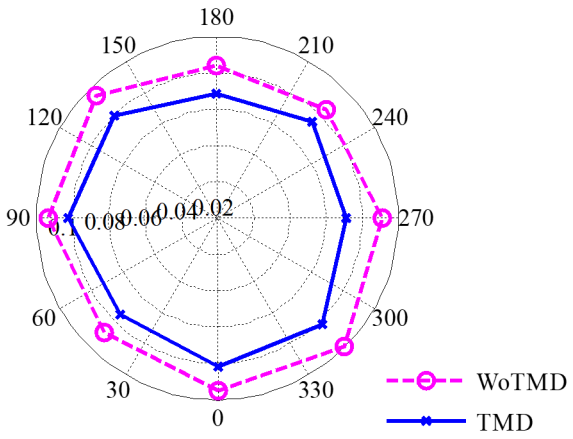

TAL_1704_Fig.11g.tif

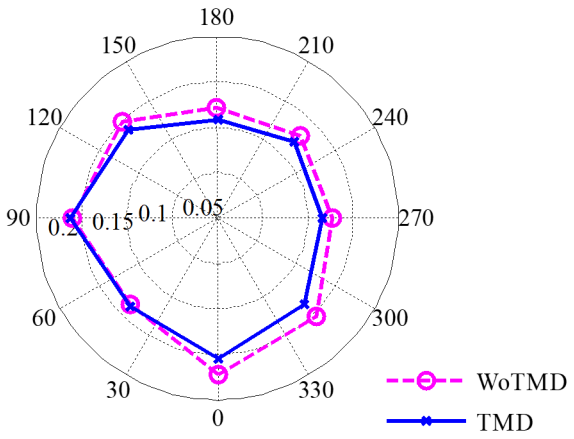

TAL_1704_Fig.11h.tif

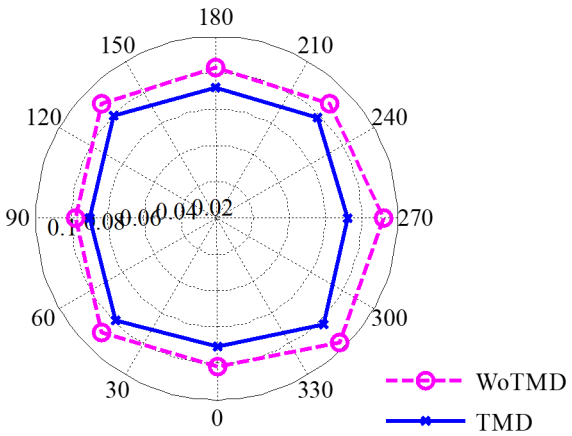

TAL_1704_Fig.11i.tif

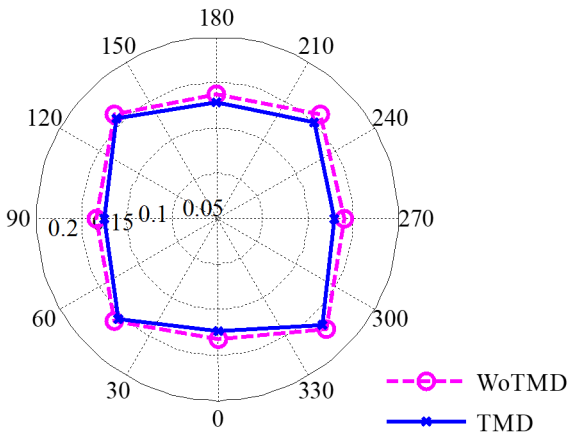

TAL_1704_Fig.11j.tif

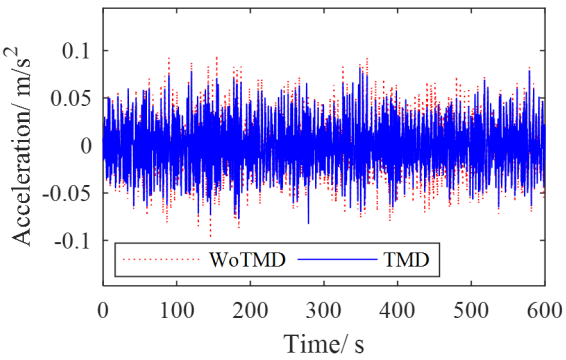

TAL_1704_Fig.12a.tif

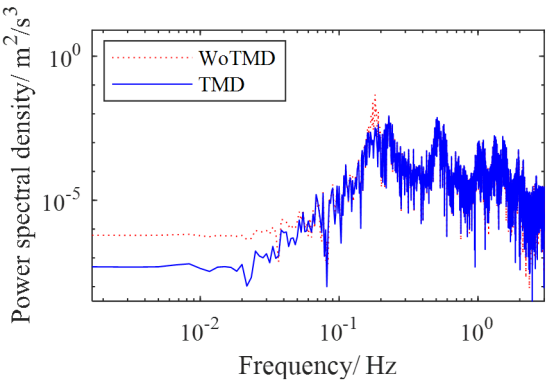

TAL_1704_Fig.12b.tif

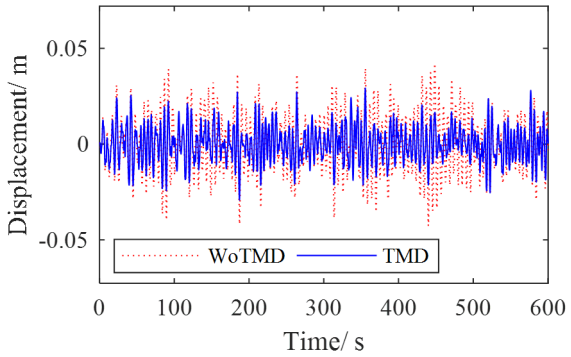

TAL_1704_Fig.12c.tif

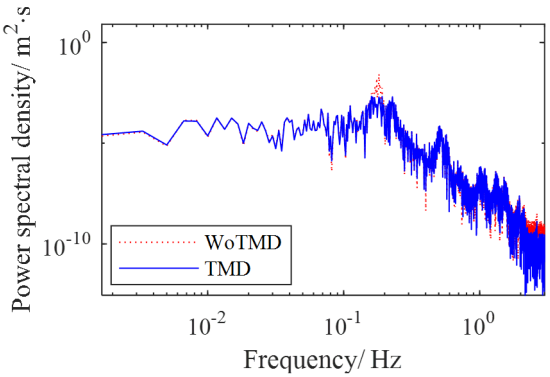

TAL_1704_Fig.12d.tif

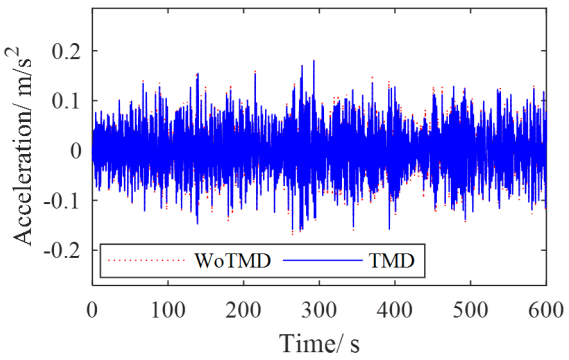

TAL_1704_Fig.13a.tif

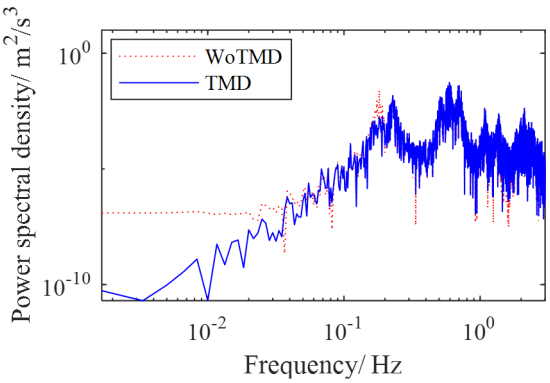

TAL_1704_Fig.13b.tif

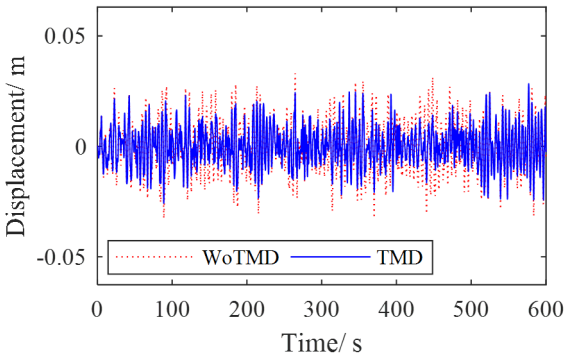

TAL_1704_Fig.13c.tif

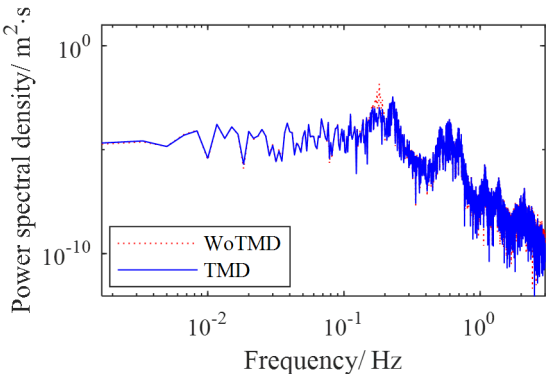

TAL_1704_Fig.13d.tif

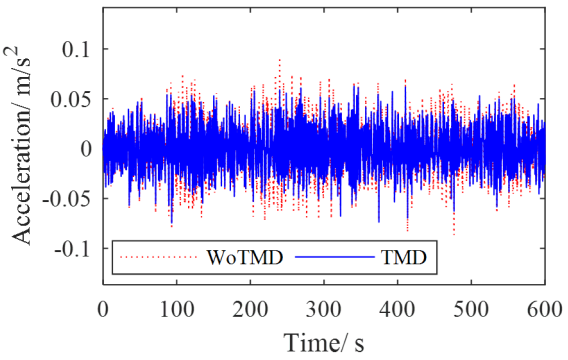

TAL_1704_Fig.14a.tif

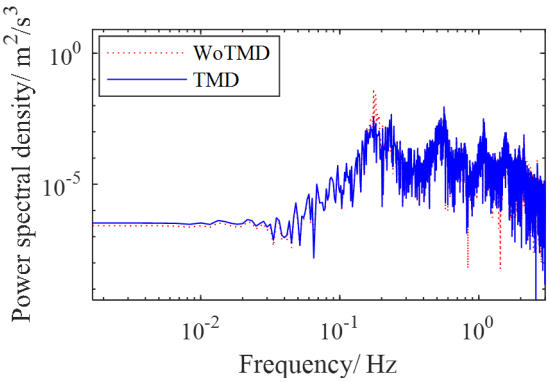

TAL_1704_Fig.14b.tif

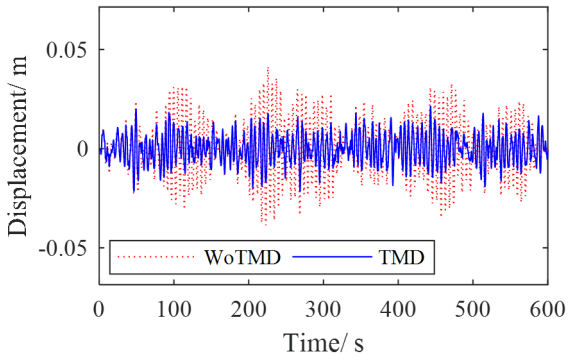

TAL_1704_Fig.14c.tif

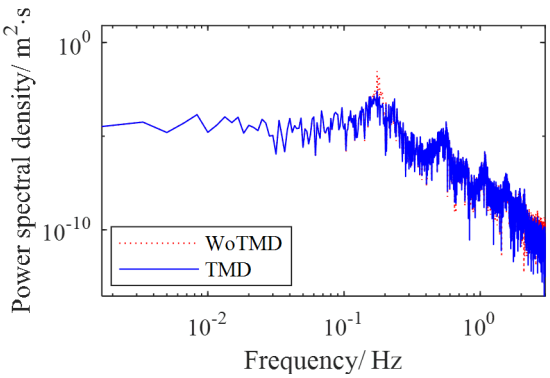

TAL_1704_Fig.14d.tif

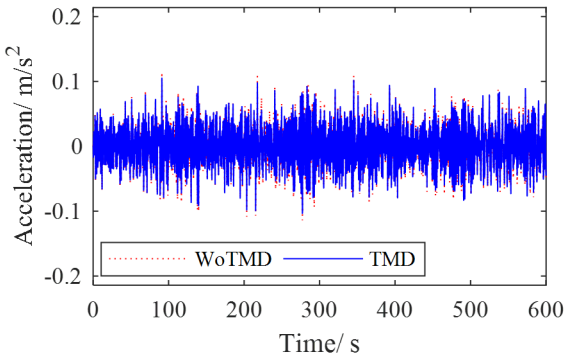

TAL_1704_Fig.15a.tif

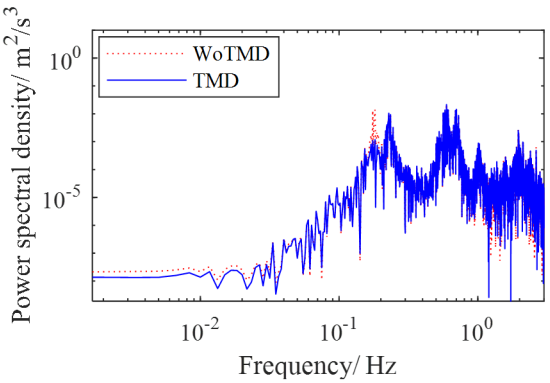

TAL_1704_Fig.15b.tif

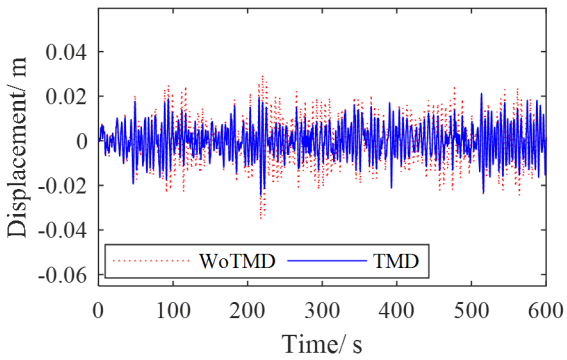

TAL_1704_Fig.15c.tif

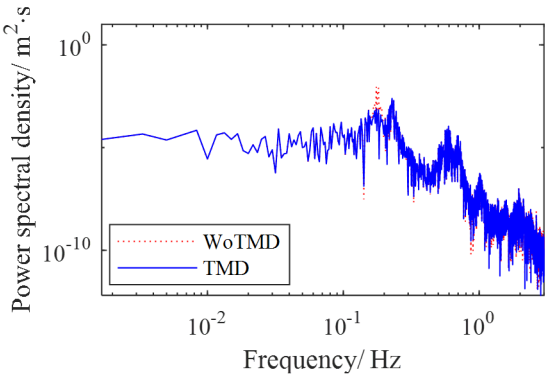

TAL_1704_Fig.15d.tif